Presented at Intl. Brazing and Soldering Conference 2006, SAND2006-2211C.

Mechanical Behavior of the 98Ag-2Zr and 97Ag-1Cu-2Zr Active Braze Alloys

John J. Stephens
Sandia National Laboratories, Albuquerque, NM, USA 87185
E-mail: jjsteph@sandia.gov

Michael K. Neilsen
Sandia National Laboratories, Albuquerque, NM, USA 87185
E-mail: mkneils@sandia.gov

Abstract

Ceramic-to-metal brazing is being simulated using finite element analysis (FEA) codes to investigate the effects of braze alloy, braze process, and geometry variations on stress levels generated during brazing. The accuracy of these simulations depends on how realistically braze material behavior is understood and modeled. A viscoplastic model for braze alloys was developed. This model uses a hyperbolic sine function of effective stress in its kinetic equation for the inelastic strain rate. Evolution equations for the internal state variables describe competing mechanisms of power-law hardening and thermal recovery. Parameters for the 98Ag-2Zr and 97Ag-1Cu-2Zr braze alloys were obtained from a combination of experiments including uniaxial compression and creep compression. This paper includes a brief description of the viscoplastic model, tables with material parameters for the 98Ag-2Zr and 97Ag-1Cu-2Zr alloys, and summary data plots for compressive stress-strain and creep tests. Stress analysis results for a typical ceramic-to-metal braze joint using 98Ag-2Zr are compared to results obtained with the 97Ag-1Cu-2Zr, and 63Ag-35.25Cu-1.75Ti braze alloys.

Introduction

Ceramic parts are used in high temperature applications due to their superior strength and wear properties compared with metals. Alumina ceramics are also used in a number of important high-voltage, vacuum, electronic components at Sandia National Laboratories. However, when ceramic parts are used there is often a need to join the ceramic part to a metal part. One of the most reliable joining methods is ceramic-to-metal brazing. During a typical ceramic-to-metal brazing process, residual stress is generated due to the differential thermal expansion of the ceramic, metal, and braze alloy. Residual stress levels generated during the brazing process depend primarily on braze joint geometry, temperature cool-down profile, and response of the joint materials [1]. The effects of variations in joint geometry, materials, or cool-down profile can be investigated using finite element analyses. However, the accuracy of these analyses is critically dependent on the validity of the constitutive models used to describe the behavior of braze joint materials. Constitutive models for the 98Ag-2Zr and 97Ag-1Cu-2Zr braze alloys are developed in this paper.

This paper begins with a brief review of existing material data [2,3,4]. Next, results from uniaxial compression and creep compression experiments on the 98Ag-2Zr and 97Ag-1Cu-2Zr alloys are shown. Then a viscoplastic constitutive model for braze alloys is presented and the process used to obtain material parameters for 98Ag-2Zr and 97Ag-1Cu-2Zr is described. Stress analysis results for a typical ceramic-to-metal braze joint using the 98Ag-2Zr alloy are compared to results obtained with the 97Ag-1Cu-2Zr, and 63Ag-35.25Cu-1.75Ti alloys.

Existing Material Data

Three different sources of useful information were found during a review of existing material data. The first was WESGO Metal's website [2]. This website provides limited data for the large variety of braze alloys that are manufactured by WESGO. Data for the 98Ag-2Zr braze alloy was not available at this site but data for pure silver obtained from this site is listed in Table 1.

Table 1. Pure Ag properties from WESGO Metals [2].

Parameter	Units	Value
Density	gm/cm^3	10.5
Young's Modulus	GPa	71
Yield Strength	MPa	54
Tensile Strength	MPa	125
Thermal Conductivity	W/(m*K)	418.7
Thermal Expansion Coefficient	1/C	20.6×10^{-6}
Electrical Resistivity	ohm*m	1770×10^{-9}
Solidus Temperature	C	960

Young's modulus for pure silver as a function of temperature was reported by Koster [3]. Poisson's rate for pure silver as a function of temperature was reported by Wawra [4]. Young's modulus and Poisson's ratio data for pure silver provided by Koster [3] and Wawra [4] was tabulated as a function of temperature in Table 2. Note that Young's modulus for pure silver provided by the Wesgo website [2] of 71 GPa is lower than the room temperature Young's modulus for pure silver given by Koster [3]. This difference may be due to differences in the measurement technique used to obtain Young's modulus. A dynamic modulus measurement will typically be higher and more accurate than a Young's modulus measurement obtained from the initial slope in a uniaxial stress-strain experiment.

Table 2. Elastic moduli for Pure Ag [3,4].

Temperature (°C)	Young's Modulus (GPa)	Poisson's Ratio
23	83.5	0.368
200	77.0	0.372
250	75.0	0.374
350	70.0	0.377
450	65.0	0.380
550	60.0	0.384
650	54.5	0.388
750	49.0	0.393

Uniaxial and Creep Compression Experiments

A series of uniaxial compression and creep compression experiments were also performed at various temperatures to investigate the elastic and inelastic response of the 98Ag-2Zr and 98Ag-1Cu-2Zr braze alloys. True stress-true strain curves obtained from the uniaxial compression experiments are shown in Figs. 1 and 2. These curves show a significant and expected large reduction in compressive strength with increases in test temperature. A comparison of Figs. 1 and 2 reveals that the 97Ag-1Cu-2Zr is stronger than the 98Ag-2Zr alloy at temperatures below 650 °C.

Minimum or steady-state creep rates obtained during the creep compression experiments on 98Ag-2Zr were examined, and two regimes of creep deformation were observed: (a) a high temperature regime, ranging from 550°C high stress tests up to 750°C, and (b) an intermediate temperature regime, ranging from 200°C up to the low stress tests at 550°C. Creep data for the high and intermediate temperature regimes are plotted in Figs. 3a and 3b, respectively. The high temperature creep regime is well fit by a classical power law creep equation

$$\dot{\varepsilon}^{ss} = 2.070 \times 10^{7} (\sigma)^{7.438} \, exp\left(\frac{-85{,}534}{R\theta}\right) \qquad (1)$$

where $\dot{\varepsilon}^{ss}$ is the minimum or steady-state creep rate (s^{-1}), σ is the applied true stress in MPa, R is the gas constant (1.987 cal/mole/Kelvin), θ is the absolute temperature in Kelvin. A correlation (r^2) of 0.904 was obtained.

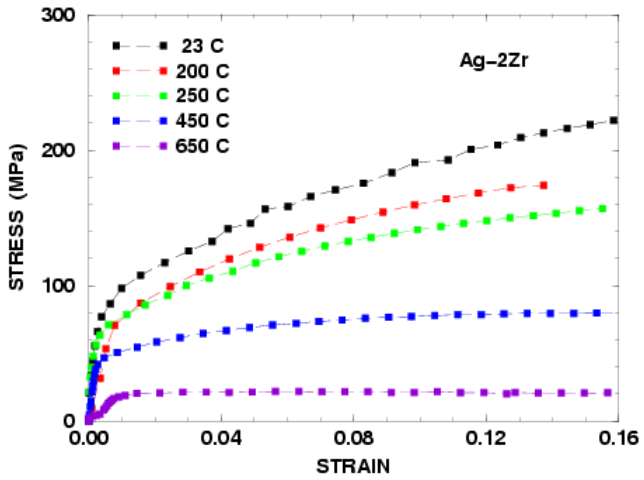

Figure 1. True stress-strain curves for 98Ag-2Zr generated by isothermal, uniaxial compression experiments. Samples were subjected to a constant true strain rate of 1.67 x 10^{-4} per second.

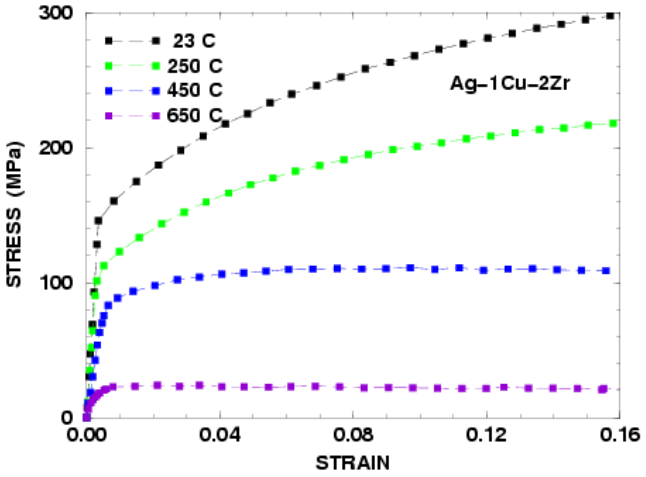

Figure 2. True stress-strain curves for 97Ag-1Cu-2Zr generated by isothermal, uniaxial compression experiments. Samples were subjected to a constant true strain rate of 1.67 x 10^{-4} per second.

The intermediate temperature creep correlation that was found to work best for the 98Ag-2Zr alloy was a Garofalo [5] type creep equation

$$\dot{\varepsilon}^{ss} = 2.950 \times 10^{6} \, sinh^{5.81}\left(\frac{\sigma}{111.}\right) exp\left(\frac{-32{,}398}{R\theta}\right) \qquad (2)$$

where $\dot{\varepsilon}^{ss}$ is again the minimum or steady-state creep rate (s^{-1}) which is given as a hyperbolic sine function of σ, the true stress in MPa. A correlation coefficient (r^2) of 0.8937 was obtained, based on the 22 data points included. This correlation is plotted in Fig. 3b.

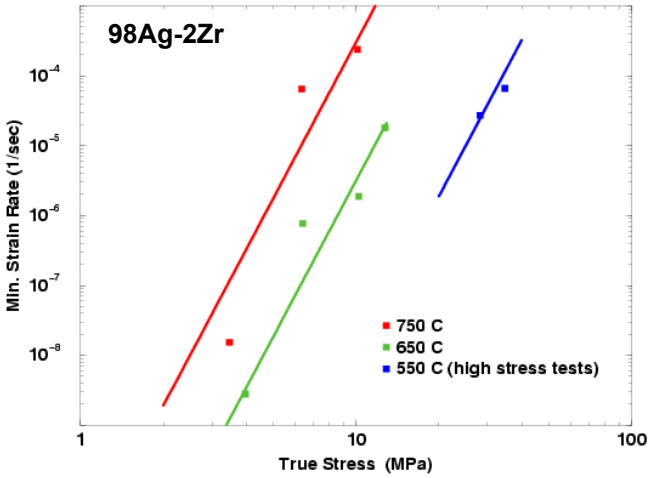

(a) High temperatures, solid lines = Equation 1 fit

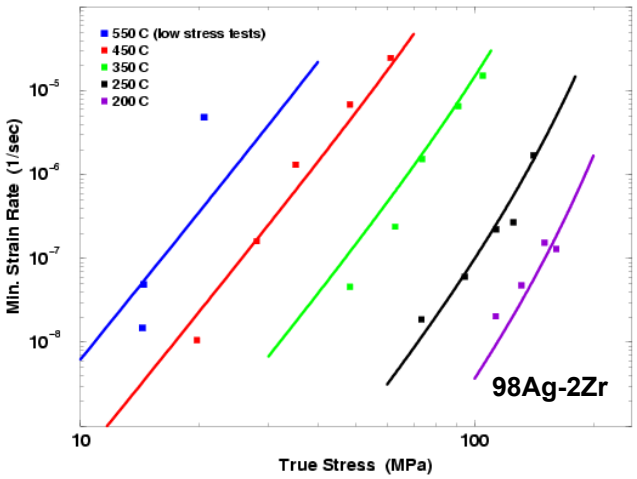

(b) Intermediate temperatures, solid lines = Equation 2 fit

Figure 3. Creep correlations for annealed 98Ag-2Zr alloy.

Creep compression experiments on 97Ag-1Cu-2Zr revealed that at temperatures of 450 and 550°C, the minimum strain rate can be represented by a power law equation as follows

$$\dot{\varepsilon}^{ss} = 6.073\times10^{8}(\sigma)^{8.694}\, exp\left(\frac{-98{,}517}{R\theta}\right) \qquad (3)$$

The creep data at 450°C and 550°C, along with the trend lines based on Equation 3, are shown in Fig. 4a. A correlation coefficient of r^2 = 0.966 was obtained from multivariable regression analysis. The stress exponent of 8.694 which is observed in Equation 3, is comparable with the high temperature stress exponent previously obtained for 98Ag-2Zr alloy (n = 7.438 in Equation 1). Also, note that the activation energy for power law creep in 97Ag-1Cu-2Zr (98,517 cal/mole) is also comparable to the results for 98Ag-2Zr (85,534 cal/mole in Equation 1).

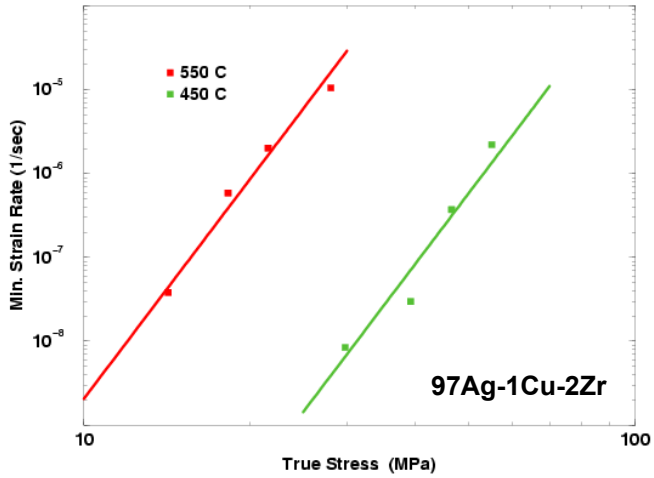

(a) High temperatures, solid lines = Equation 3 fit

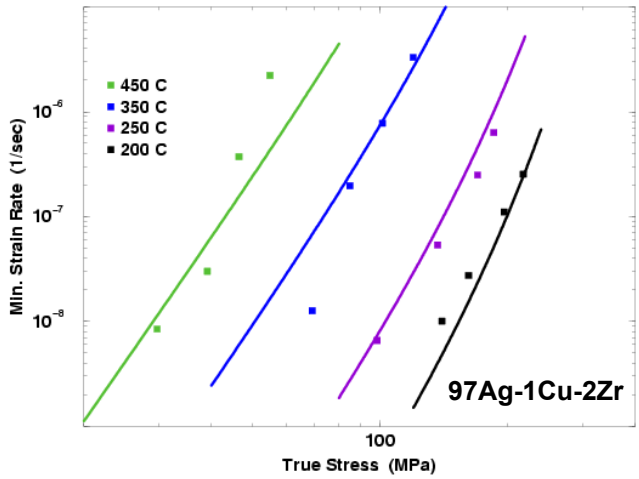

(b) Intermediate temperatures, solid lines = Equation 4 fit

Figure 4. Creep correlations for annealed 98Ag-1Cu-2Zr.

The Garofalo sinh equation [5] also represented the best intermediate temperature fit (200 to 450°C) for creep of the 98Ag-1Cu-2Zr alloy.

$$\dot{\varepsilon}^{ss} = 3.638\times10^{4}\, sinh^{5.742}\left(\frac{\sigma}{131.}\right) exp\left(\frac{-29{,}228}{R\theta}\right) \qquad (4)$$

where $\dot{\varepsilon}^{ss}$ is again the minimum or steady-state creep rate (s^{-1}) which is given as a hyperbolic sine function of σ, the applied true stress in MPa. Equation 4 is based on 16 data points, and has a correlation coefficient r^2 = 0.858 (Figure 4b). It is interesting that the 450°C data are fit well by both

Equations 3 and 4. This suggests that 450°C is a boundary temperature between the two creep regimes. The apparent stress exponent observed for 97Ag-1Cu-2Zr (n' = 5.742) is close to the value observed for 98Ag-2Zr alloy (n' = 5.81). A similar observation applies for the creep activation energy for the ternary alloy (Q = 29,228 cal/mole) compared with the activation energy for the binary 98Ag-2Zr alloy (Q = 32,398 cal/mole).

In general, there is an increase in creep strength for the 97Ag-1Cu-2Zr alloy relative to the 98Ag-2Zr alloy. This is shown in Fig. 5 for a temperature of 250°C. The applied stress required to achieve the same minimum strain rate is about 40 percent higher for 97Ag-1Cu-2Zr relative to the 98Ag-2Zr alloy. The stress required to produce significant creep deformation in the ternary alloy is still consistent with the requirement for a braze alloy with excellent capability for stress relaxation. Braze alloys with significant capacity for stress relaxation are desirable for reducing stress levels generated in brittle ceramic materials during ceramic-to-metal brazing.

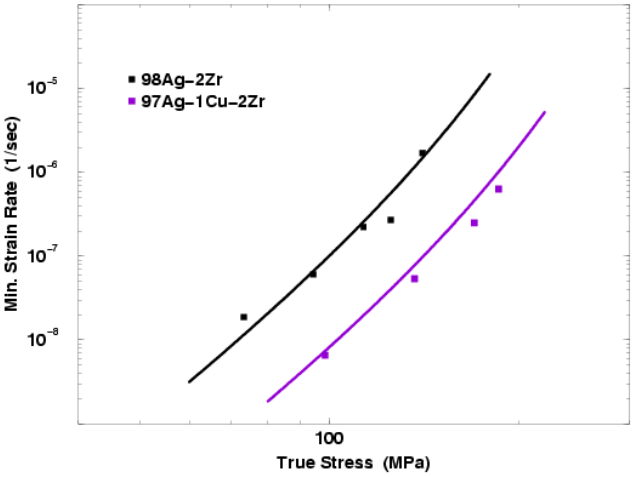

Figure 5. Comparison of the 250 °C steady state creep data for 98Ag-2Zr with the same creep data for 97Ag-1Cu-2Zr alloy.

Viscoplastic Braze Model

Based on the experiments presented in the previous section, a viscoplastic model was developed to describe the elastic, creep, and plastic deformation of the 98Ag-2Zr and 97Ag-1Cu-2Zr alloys. Since a hyperbolic sine function of applied stress worked well to describe the steady-state creep response of these alloys, the viscoplastic model was developed using a kinetic equation for the inelastic strain rate, $\boldsymbol{\varepsilon}^{in}$, with the following form:

$$\boldsymbol{\varepsilon}^{in} = \frac{3}{2}\gamma \mathbf{n} = \frac{3}{2} f \ \sinh^{p}\left(\frac{\tau}{D}\right)\mathbf{n} \tag{5}$$

where γ is a scalar measure of the inelastic strain rate, f is a function of temperature, D is an internal state variable which accounts for isotropic hardening and recovery, $\mathbf{n}$ is the normalized stress difference tensor which is given by,

$$\mathbf{n} = \frac{\mathbf{s} - \frac{2}{3}\mathbf{B}}{\tau} \tag{6}$$

where $\mathbf{s}$ is the stress deviator, $\mathbf{B}$ is the second-order state tensor which accounts for kinematic hardening and recovery, and τ is a scalar measure of the stress difference magnitude as follows

$$\tau = \sqrt{\frac{3}{2}\left(\mathbf{s} - \frac{2}{3}\mathbf{B}\right) : \left(\mathbf{s} - \frac{2}{3}\mathbf{B}\right)} \tag{7}$$

Competing non-linear hardening and thermal recovery mechanisms are captured by the evolution equations for the internal state variable D and the internal state tensor $\mathbf{B}$. Evolution of the internal state variable D is given by

$$\dot{D} = \frac{A_1 \gamma}{(D - D_0)^{A_3}} - A_2 (D - D_0)^2 \tag{8}$$

where D_0, A_1, A_2, and A_3 are material parameters. Evolution of the second-order state tensor $\mathbf{B}$ is given by

$$\dot{\mathbf{B}} = \frac{A_4 \mathbf{d}^{in}}{b^{A_6}} - A_5 b \mathbf{B} \tag{9}$$

where A_4, A_5, and A_6 are material parameters and b is the magnitude of $\mathbf{B}$ as follows

$$b = \sqrt{\frac{2}{3}\mathbf{B} : \mathbf{B}} \tag{10}$$

Parameters for 98Ag-2Zr and 97Ag-1Cu-2Zr

Selection of material parameters for viscoplastic constitutive models can be quite complex [6]. Parameters for the 98Ag-2Zr and 97Ag-1Cu-2Zr braze alloys were obtained from a non-linear least squares fit to the uniaxial compression data presented in Figs. 1 and 2 and the creep compression data. The non-linear least squares fit to this data was performed using the Levenberg and Marquardt Nonlinear Least Squares Algorithm [7] and a driver program for the viscoplastic braze model that had been developed and used previously to obtain material parameters for the 63Ag-35.25Cu-1.75Ti alloy [8]. Young's modulus data generated by Koster [3] and Poisson's

ratio data published by Wawra [4] were used as input to this fitting process. Also, initial estimates for the material parameters were based on the steady state creep correlations presented in the previous section.

Material parameters obtained from the non-linear least squares fitting process are summarized in Tables 3 and 4. Since, the uniaxial and creep compression data was monotonic, separation of kinematic hardening and recovery from isotropic hardening and recovery was not possible. For the fits tabulated here, purely isotropic hardening and recovery was assumed.

Table 3. 98Ag-2Zr Material Parameters.

Temp. (°C)	Flow Rate ln(f)	Sinh Expo. p	Isotropic Hardening, A_1 (MPa^{A3+1})	Isotropic Recov., A_2 1/(MPa-sec)
23	-86.29	12.0	15840.	2.117e-11
200	-71.11	11.4	12300.	2.000e-10
250	-64.10	11.26	12290.	8.469e-8
350	-37.15	5.81	3933.	3.191e-7
450	-30.36	5.81	3245.	9.641e-6
550	-24.59	5.81	3100.	2.541e-4
650	-18.12	5.81	3087.	6.457e-3
750	-10.67	5.81	3000.	7.116e-3
Iso. Exponent, A_3			1.7278	
Kin. Harden.,A_4 (MPa^{A6+1})			0.0	
Kin. Rec., A_5 1/(MPa-sec)			0.0	
Kin. Exponent, A_6			1.7278	
Flow Stress, D_0 (MPa)			5.00	

Table 4. 98Ag-1Cu-2Zr Material Parameters.

Temp. (°C)	Flow Rate ln(f)	Sinh Expo. p	Isotropic Hardening, A_1 (MPa^{A3+1})	Isotropic Recov., A_2 1/(MPa-sec)
23	-49.47	18.0	14.09e6	1.00e-10
200	-48.76	17.0	5.81e6	3.13e-9
250	-46.64	15.0	2.59e6	3.82e-8
350	-43.63	10.73	2.26e6	1.27e-6
450	-24.77	5.742	0.105e6	4.82e-5
550	-15.17	5.742	60.0e3	8.14e-5
650	-8.949	5.742	25.0e3	1.46e-4
750	-2.720	5.742	8.0e3	5.00e-4
Iso. Exponent, A_3			2.557	
Kin. Harden.,A_4 (MPa^{A6+1})			0.0	
Kin. Rec., A_5 1/(MPa-sec)			0.0	
Kin. Exponent, A_6			2.557	
Flow Stress, D_0 (MPa)			15.00	

Simulation of Uniaxial Compression Tests

The uniaxial compression experiments were simulated using the viscoplastic model and the material parameters for the 98Ag-2Zr alloy listed in Table 3 and material parameters for the 98Ag-1Cu-2Zr alloy listed in Table 4. Results from these simulations are shown in Fig. 6. As expected, the model predictions match the experimental measurements well. Also, this figure clearly shows the models ability to capture the dramatic change in compressive strength with changes in temperature.

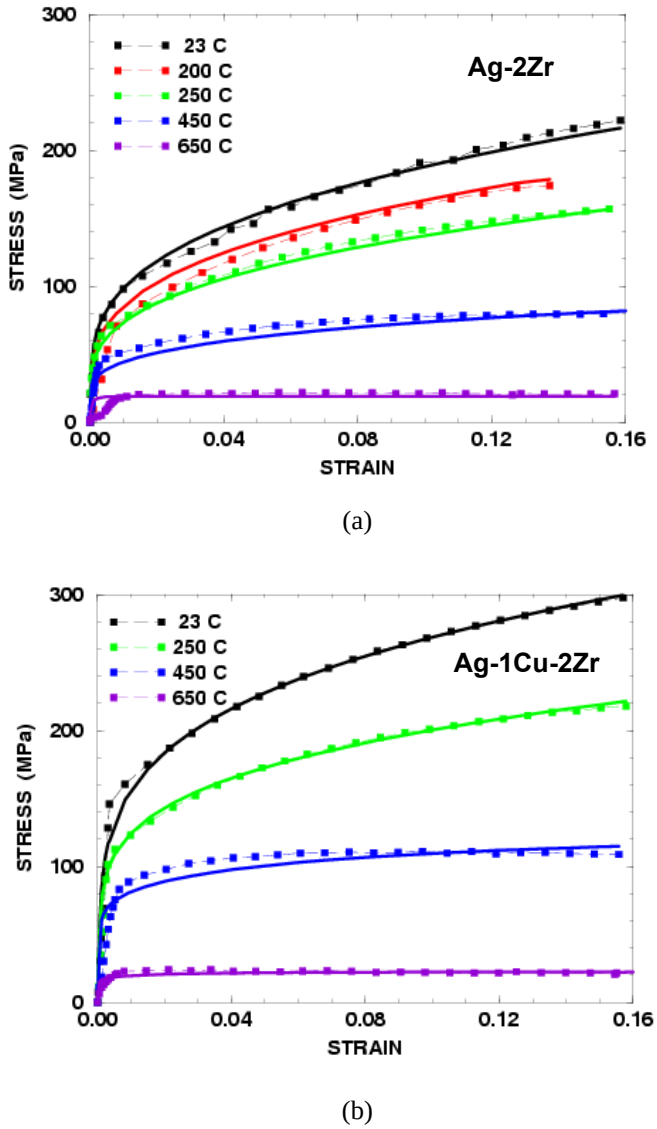

Figure 6. True stress-strain curves generated by constant rate, isothermal, uniaxial compression experiments compared with viscoplastic model predictions for (a) 98Ag-2Zr and (b) 97Ag-1Cu-2Zr. Symbols represent experiments and solid lines represent model predictions.

Simulation of Creep Compression Tests

Next, several creep compression experiments at temperatures of 250 °C, 450 °C, and 650 °C were simulated. In these experiments, the applied axial load or engineering stress was ramped to a specified value and held constant for the duration of the test and the resulting axial strain history was measured. In the simulations, the applied engineering stress was also ramped to the same specified value and the resulting strain history was plotted. A comparison of experimental and predicted strain histories indicates that the model matches the experimental data well for most applied engineering stress and temperature levels (Figure 7).

The largest discrepancies between model prediction and experimental measurement are for the low-stress, long-duration, 650 °C experiments in which an engineering stress of 8 or 12 MPa is applied (Figure 7c). The unexpected reduction in creep rate observed during these experiments is most likely caused by internal oxidation of the Zr addition during the extended hold at elevated temperature in an air environment. This experimentally observed behavior is not likely during a brazing operation because the atmosphere will be controlled. At the present time, all of the brazing operations conducted with 98Ag-2Zr utilize a dry hydrogen, i.e. reducing atmosphere.

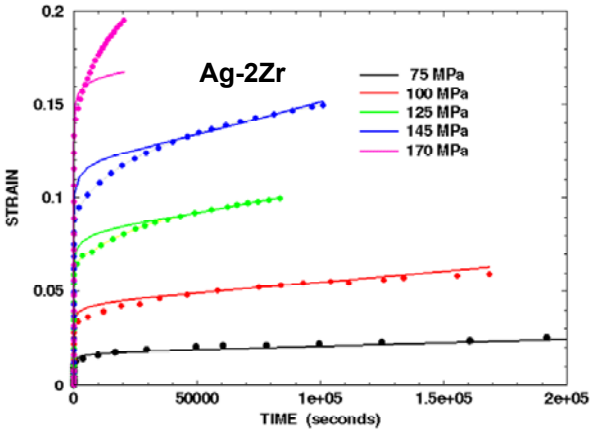

(a) 98Ag-2Zr, 250 °C

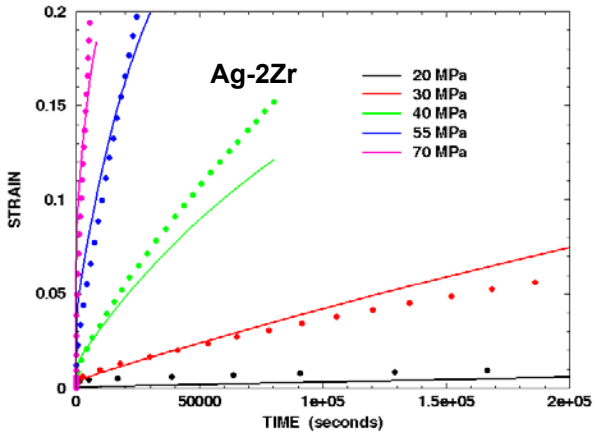

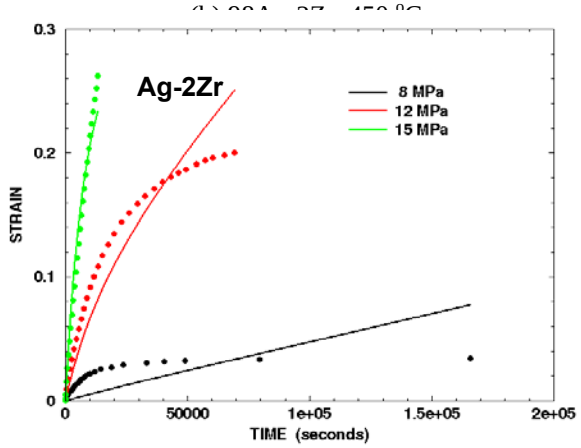

(c) 98Ag-2Zr, 650 °C

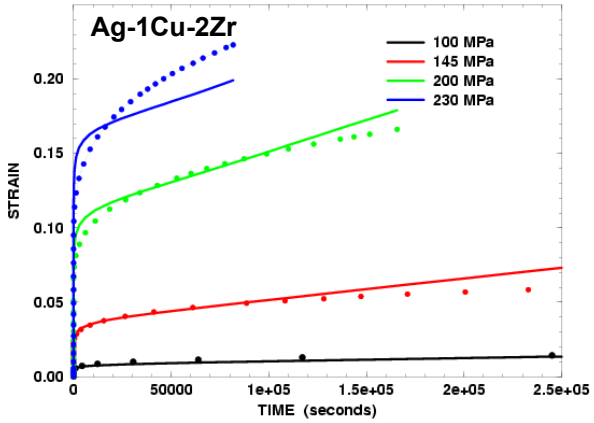

(d) 97Ag-1Cu-2Zr, 250 °C

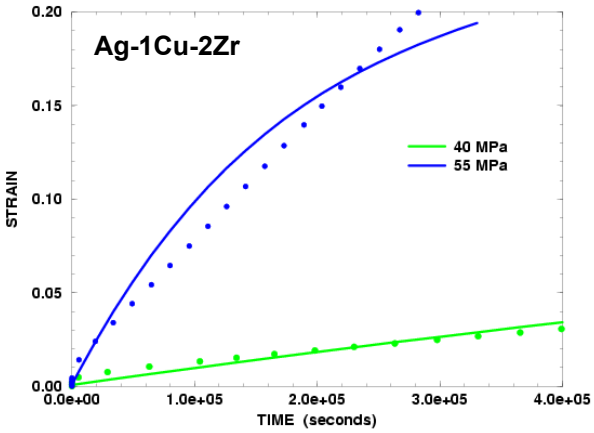

(e) 97Ag-1Cu-2Zr, 650 °C

Figure 7. *True strain history curves generated by constant applied load, creep compression experiments. Dashed lines show experimental results and solid lines show viscoplastic model predictions. Legend shows the applied engineering stress level.*

Simulation of Ceramic-to-Metal Brazing

Finally, the ceramic-to-metal brazing of an alumina ceramic rod to an Fe-Ni-Co alloy rod with 98Ag-2Zr, 97Ag-1Cu-2Zr, or 63Ag-35.25Cu-1.75Ti was simulated using the viscoplastic model. These simulations were performed using the two-dimensional finite element model shown in Fig. 8. The alumina ceramic and Fe-Ni-Co alloy rods have a 6.0 mm diameter and a 6.0 mm height. The braze layer has a 0.127 mm thickness. The alumina ceramic was modeled as an elastic material with a Young's modulus of 303.4 GPa and a Poisson's ratio of 0.22. The iron-nickel-cobalt alloy was modeled as an elastic material with a Young's modulus of 137.9 GPa and a Poisson's ratio of 0.317. Material parameters for the 98Ag-2Zr and 97Ag-1Cu-2Zr alloys are listed in Tables 2, 3, and 4. Material parameters for the 63Ag-35.25Cu-1.75Ti alloy were obtained from [8]. A plot of thermal strain as a function of temperature (Fig. 9) shows that the braze alloys have a much higher thermal expansion coefficient than either the alumina ceramic or the Fe-Ni-Co alloy. The finite element model was assumed stress free at the braze solidus temperature (960 ^{o}C for 98Ag-2Zr and 97Ag-1Cu-2Zr, and 780 ^{o}C for 63Ag-35.25Cu-1.75Ti). The finite element model was then cooled to room temperature in one hour and the resulting stress distributions were investigated.

Results from the simulation with the 97Ag-1Cu-2Zr braze showed that a maximum tensile stress of 45.4 MPa would be generated on the alumina ceramic surface at Point A and a residual tensile stress of only 6.62 MPa would remain at Point A upon completion of the brazing process (Fig. 10). A residual tensile stress of 46.1 MPa is generated on the alumina to braze interface (Point B in Fig. 10). The simulation with the 98Ag-2Zr braze indicated that a maximum tensile stress of 28.3 MPa would be generated on the alumina ceramic surface at Point A and that a residual tensile stress of only 7.81 MPa would remain at Point A upon completion of the brazing process (Fig. 11). A residual tensile stress of 50.8 MPa is generated on the alumina to braze interface (Point B in Fig. 10) with the 98Ag-2Zr braze. Thus, the 97Ag-1Cu-2Zr braze generated a higher tensile stress on the surface of the ceramic during the brazing process but lower residual tensile stress than the 98Ag-2Zr braze.

The simulation with the 63Ag-35.25Cu-1.75Ti braze indicated that a maximum tensile stress of 52.3 MPa would be generated on the alumina ceramic surface at Point A and that a residual tensile stress of only 15.9 MPa would remain at Point A upon completion of the brazing process (Fig. 11). A residual tensile stress of 36.8 MPa is generated on the alumina to braze interface (Point B in Fig. 10) with 63Ag-35.25Cu-1.75Ti braze. Although the 63Ag-35.25Cu-1.75Ti alloy has a lower melting point than either of the two Ag-Zr alloys, the segregation and strengthening effect of Ti in the Cu-rich phase produces a significant increase in residual stresses. Figures 1 and 7 in a related paper [9] in this volume illustrate the greater creep strength of the 63Ag-35.25Cu-1.75Ti relative to the other two alloys discussed in this paper.

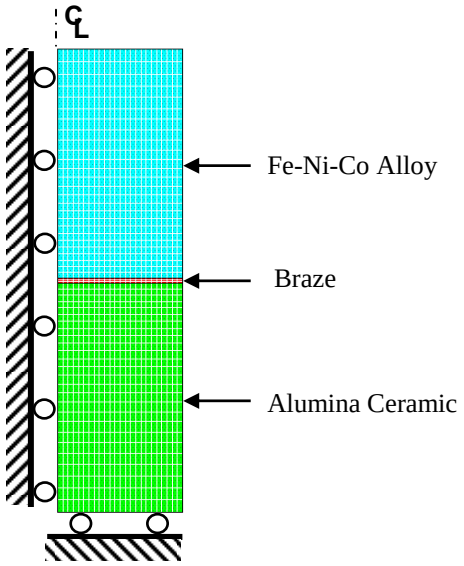

Figure 8. Axisymmetric finite element model used in the brazing simulations.

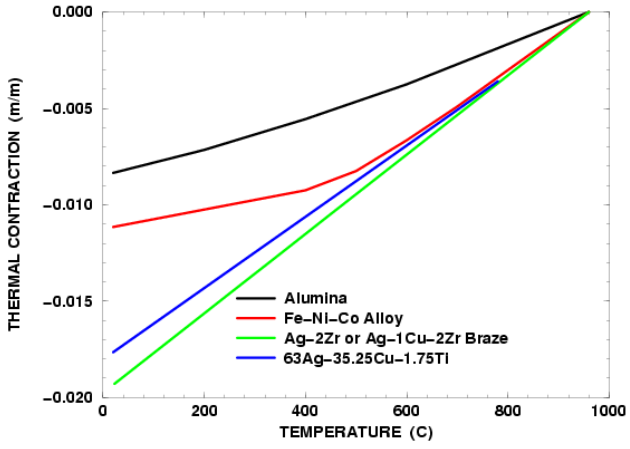

Figure 9. Thermal expansion of materials used in the ceramic-to-metal brazing simulations.

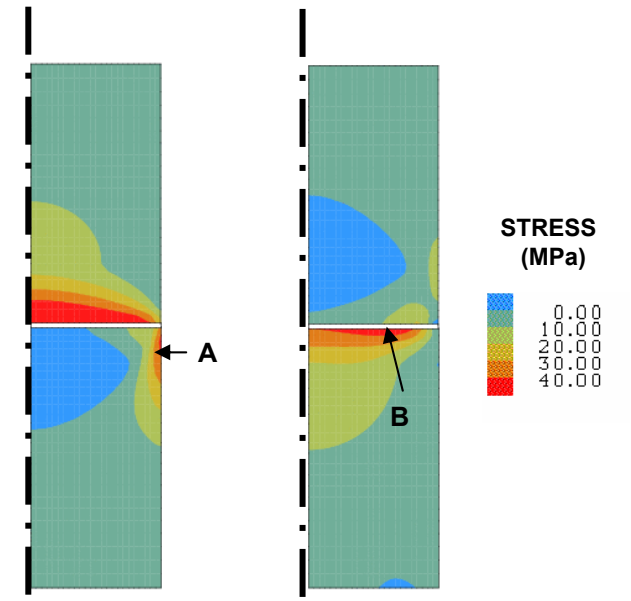

a. 1800 seconds (490 °C) b. 3600 seconds (23 °C)

Figure 10. Maximum tensile stress generated in alumina ceramic during the braze process with 97Ag-1Cu-2Zr braze.

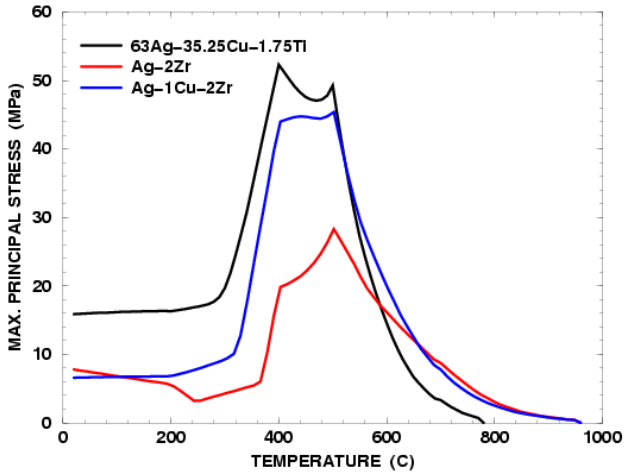

Figure 11. Maximum tensile stress generated at Point A in alumina ceramic during the braze process with 63Ag-35.25Cu-1.75Ti, 98Ag-2Zr, and 97Ag-1Cu-2Zr braze alloys.

Summary

A viscoplastic braze model has been developed for the 98Ag-2Zr and a new 98Ag-1Cu-2Zr braze alloys. This model can be used to simulate ceramic-to-metal brazing and subsequent environmental heating or cooling. Material parameters for this new model are based on results from a combination of uniaxial compression and creep compression experiments which were performed at a variety of temperatures between 23 °C and 750 °C, inclusively. In the future, cyclic loading experiments should be completed at a variety of temperatures to allow for the modeling of both isotropic and kinematic hardening and recovery. The current parameters assume that the hardening and recovery is purely isotropic.

The new model was used to simulate the ceramic-to-metal brazing of an alumina ceramic rod to a Fe-Ni-Co alloy rod with 98Ag-2Zr, 97Ag-1Cu-2Zr and 63Ag-35.25Cu-1.75Ti. The interesting result from these simulations was that the predicted peak and residual tensile stress on the outside surface of the ceramic was actually highest when the lower temperature 63Ag-35.25Cu-1.75Ti braze alloy was used. The transient peak tensile stress on the surface of the ceramic was lowest when the 98Ag-2Zr braze alloy was used.

Acknowledgement

Sandia is a multi-program laboratory operated by Sandia Corporation, a Lockheed Martin Company, for the United States Department of Energy's National Nuclear Security Administration under contract DE-AC04-94AL85000. Sandia National Laboratories program and engineering support of this work is gratefully acknowledged.

References

[1] Stephens, J.J., Burchett, S.N., and Hosking, F.M., "Residual Stresses in Metal Ceramic Brazes: Effect of Creep on Finite Element Analysis Results," Metal-Ceramic Joining, Edited by P. Kumar and V.A. Greenhut, (The Minerals, Metals & Materials Society, 1991)

[2] Wesgo Metals Website, braze alloy physical data page, http://www.wesgometals.com/physdata.html, (2005

[3] Koster, W., *Z. Metallk.* Vol. 39, (1948), pp. 145.

[4] Wawra, H. "Kroner-Limits of Elastic Moduli of materials of Technical Importance. Part II: Elastic Moduli of Elements as a Function of Temperature," *Z. Metallk.*, Vol. 69, (1978), pp. 518-523.

[5] Garofalo, F., Fundamentals of Creep and Creep-Rupture in Metals, (The MacMillan Company, New York, 1965).

[6] Fossum, A.F., "Parameter Estimation for an Internal Variable Model Using Nonlinear Optimization and Analytical/Numerical Response Sensitivities," Journal of Engineering Materials and Technology, Vol. 119., (1997), pp. 337-345.

[7] More, J.J., "The Levenberg-Marquardt Algorithm: Implementation and Theory," Lecture Notes in Mathematics 630, Edited by G.A. Watson, (Springer-Verlag, 1978).

[8] Neilsen, M.K., Burchett, S.N., Stone, C.M., and Stephens, J.J., "A Viscoplastic Theory for Braze Alloys," SAND96-0894, (Sandia National Laboratories, 1996).

[9] Stephens, J.J., Hosking, F.M., Walker, C.A., Dudley, E. and Yost, F.G., "The Evolution of a Ternary Ag-Cu-Zr Active Braze Filler Metal for Kovar/Alumina Braze Joints," in this volume.